

Multi-Agent Reinforcement Learning Scheduling to Support Low Latency in Teleoperated Driving

Giacomo Avanzi, Marco Giordani, Michele Zorzi

Department of Information Engineering, University of Padova, Italy.

Email: {giacomo.avanzi, marco.giordani, michele.zorzi}@dei.unipd.it

Abstract—The teleoperated driving (TD) scenario comes with stringent Quality of Service (QoS) communication constraints, especially in terms of end-to-end (E2E) latency and reliability. In this context, Predictive Quality of Service (PQoS), possibly combined with Reinforcement Learning (RL) techniques, is a powerful tool to estimate QoS degradation and react accordingly. For example, an intelligent agent can be trained to select the optimal compression configuration for automotive data, and reduce the file size whenever QoS conditions deteriorate. However, compression may inevitably compromise data quality, with negative implications for the TD application. An alternative strategy involves operating at the Radio Access Network (RAN) level to optimize radio parameters based on current network conditions, while preserving data quality. In this paper, we propose Multi-Agent Reinforcement Learning (MARL) scheduling algorithms, based on Proximal Policy Optimization (PPO), to dynamically and intelligently allocate radio resources to minimize E2E latency in a TD scenario. We evaluate two training paradigms, i.e., decentralized learning with local observations (IPPO) vs. centralized aggregation (MAPPO), in conjunction with two resource allocation strategies, i.e., proportional allocation (PA) and greedy allocation (GA). We prove via ns-3 simulations that MAPPO, combined with GA, achieves the best results in terms of latency, especially as the number of vehicles increases.

Index Terms—Teleoperated driving (TD), Predictive Quality of Service (PQoS), Multi-Agent Reinforcement Learning (MARL), Proximal Policy Optimization (PPO).

I. INTRODUCTION

In sixth generation (6G) networks, massive amounts of data will be exchanged, with human communication accounting only for a minimal fraction of the traffic [1]. Notably, vehicular communication is expected to be a key protagonist of 6G, interconnecting vehicles with other vehicles, infrastructures, pedestrians, and networks. However, fully autonomous driving with no human interaction presents critical technical challenges [2]. Therefore, the research community is focusing on teleoperated driving (TD), where a remote driver controls the vehicles based on measurements and observations generated by onboard sensors, such as high-resolution videocameras and Light Detection and Ranging (LiDAR) sensors.

The performance of the TD application strongly depends on the network conditions in which the vehicles are deployed. In particular, strict requirements must be satisfied in terms

of Quality of Service (QoS). According to 5G Automotive Association (5GAA) specifications, the service-level latency with the remote driver depends on the automation level and, for TD, should not exceed 50 ms in both uplink (UL) and downlink (DL), while reliability ranges from 99% to 99.999% [3]. However, transmitting large volumes of data may require bit rates of hundreds of megabits per second [4], and ultimately create network congestion. Moreover, unanticipated channel degradation may lead to critical safety risks and/or reliability issues for TD applications.

For this reason, Predictive Quality of Service (PQoS) was introduced as a mechanism to forecast and communicate potential QoS changes in the network, and undertake proper countermeasures to react accordingly [5]. Notably, PQoS can be based on Neural Networks (NNs), leveraging input features related to network conditions, resource availability, predicted mobility patterns, and/or other observations. Recently, Reinforcement Learning (RL) methods have been also investigated to implement PQoS in TD scenarios. For example, in our previous works [6], [7], we proposed a PQoS framework to select the optimal compression level for LiDAR data to minimize the end-to-end (E2E) latency. A Double Deep Q-Network (DDQN) model was used as the predictor, even though in [8] we explored several other RL alternatives. However, compression might inevitably degrade the quality of the LiDAR data, and possibly compromise TD operations such as object detection and recognition.

PQoS can also dynamically optimize Radio Access Network (RAN) parameters, such as the transmission power, the numerology, or the communication spectrum, based on QoS estimates [5]. An advantage of this approach is that it focuses exclusively on network-level parameters, thereby preserving the integrity and quality of the transmitted data compared to other methods that rely on, for example, compression. Notably, the RAN can be optimized at the scheduling level, e.g., based on the temporal evolution of the communication channel and the available resources. In fact, existing 5G schedulers, such as Round Robin (RR), proportional fair, earliest-deadline first, were not designed to handle time-sensitive traffic. In turn, Deep Reinforcement Learning (DRL), along with its multi-agent extension, has emerged as a powerful tool to schedule resources in a time-varying and unpredictable environment like in vehicular networks [9]. In [10], the authors proposed a new scheduler implementing a knowledge-based DRL algorithm to deal with time-sensitive traffic in 5G networks. A similar

This work was supported by the European Union under the Italian National Recovery and Resilience Plan (NRRP) Mission 4, Component 2, Investment 1.3, CUP C93C22005250001, partnership on “Telecommunications of the Future” (PE00000001 - program “RESTART”)

strategy, also based on DRL, was proposed in [11] to support Ultra-Reliable Low Latency Communication (URLCC).

Along these lines, in this paper we propose, implement, and evaluate novel Multi-Agent Reinforcement Learning (MARL) algorithms to optimize QoS (specifically, minimize the E2E latency in a TD scenario), without compromising the accuracy of data. Our approach operates at the RAN level by training local agents that optimize scheduling based on latency conditions and the available network capacity. Specifically, we investigate two extensions of the Proximal Policy Optimization (PPO) algorithm: Independent PPO (IPPO), where we optimize multiple decentralized independent agents using local observations, and Multi-Agent PPO (MAPPO), where a single centralized model is trained using data from all local agents. Moreover, we compare a Proportional Allocation (PA) approach, in which resources are distributed fairly based on some priority levels, and a Greedy Allocation (GA) approach where the available resources are assigned to the vehicle experiencing the most severe latency, at the expense of others. The algorithms are evaluated via ns-3 simulations as a function of the number of vehicles and the size of the transmitted data. The results demonstrate that MAPPO, combined with GA, gives the best results in terms of latency, and can maximize the number of vehicles that satisfy latency constraints.

The rest of the paper is organized as follows. In Sec. II we describe our system model. In Sec. III we present our MARL resource allocation algorithms. In Sec. IV we illustrate our main simulation results. In Sec. V we conclude the paper with suggestions for future work.

II. SYSTEM MODEL

In this section we describe our simulation scenario (Sec. II-A) and optimization framework (Sec. II-B).

A. Simulation Scenario

Our simulation scenario, based on [6], consists of a Next Generation Node Base (gNB), a remote host (i.e., the tele-operator or driving software), N vehicles (i.e., the User Equipments (UEs)), and the following modules.

a) Network: A wired channel interconnects the remote host with the gNB. The gNB communicates with the vehicles via the 5G New Radio (NR) protocol stack, which is simulated based on the open-source `mmwave` module for ns-3 [12].

b) Channel and mobility model: The mobility of the vehicles is simulated in Simulation of Urban MObility (SUMO) [13], in an area of the city of Bologna. The wireless channel and the propagation loss model are computed via the GEMV2 simulator [14], and channel traces are parsed in ns-3 to compute the received power.

c) Application data: Each vehicle is equipped with a User Datagram Protocol (UDP) application transmitting LiDAR point clouds at a frame rate f .¹ Data is eventually compressed by Google Draco [15]. Specifically, this software

defines several compression configurations based on the number of quantization bits $q \in \{1, \dots, 31\}$ and the number of compression levels $c \in \{0, \dots, 10\}$.

d) RAN-AI: The RAN-AI entity [16] is an intelligent network controller, installed in the gNB. Specifically, it collects measurements and metrics from the RAN (e.g., E2E latency, Signal to Interference plus Noise Ratio (SINR), etc.), and optimizes network operations to satisfy QoS constraints. In our previous work, the RAN-AI was trained based on a single centralized [6] or decentralized [8] RL agent. Rather, in this paper we study and implement different multi-agent RL solutions, as described in Sec. III.

B. Optimization Framework

PQoS aims at anticipating communication impairments and taking proper countermeasures to avoid service degradation [5]. At the RAN level, these countermeasures include, for example, adjusting data compression to reduce network congestion, adapting the periodicity and speed of data transmissions to ensure service reliability, and/or modifying vehicle speed and trajectory based on route predictions and conditions. While our previous work focused on the application layer, in this paper we operate at the scheduler level, and optimize radio resource allocation to minimize the E2E latency.

We exploit the flexibility of the frame structure in 5G networks. According to the NR standard, the available time resources are arranged into frames of 10 ms, each of which consists of 10 subframes of 1 ms and a number of slots that depends on the selected numerology [17]. Each slot consists of 14 Orthogonal Frequency Division Multiplexing (OFDM) symbols, assuming normal Cyclic Prefix (CP), whose duration also depends on the numerology. In 5G NR with Time Division Multiple Access (TDMA), dynamic downlink scheduling occurs at the OFDM symbol level, meaning that the scheduler can assign radio resources with the granularity of individual OFDM symbols within a time slot, rather than that of the full slot or the subframe as in 4G LTE. The RAN-AI entity, described in Sec. II-A, implements an MARL algorithm that determines the optimal number of resources, i.e., OFDM symbols, to be allocated to each UE for transmission.

Channel resources are limited, and all UEs compete for those resources to satisfy latency constraints. Notably, radio resource allocation is governed by a priority level parameter $k \in \{1, \dots, K\}$, which is related to the network conditions of a given UE. Hence, lower-priority UEs ($k \rightarrow 1$) receive fewer resources, as latency requirements are easier to satisfy, while higher-priority UEs ($k \rightarrow K$) require more resources. The number of priority levels K defines the granularity of the agent's decision. We consider two scheduling methodologies, namely a proportional and a greedy approach (as described in Sec. III). A baseline RR scheduler is used as our benchmark.

III. PROPOSED MARL SCHEDULING ALGORITHM FOR TD

RL is a machine learning (ML) technique where an agent interacts with the environment to learn how to maximize a

¹While future teleoperated cars will be equipped with several types of sensors, including radar, camera and LiDAR sensors, in this work, without loss of generality, we focus on the transmission of LiDAR perceptions.

cumulative future reward. The RL framework can be formalized mathematically as a Markov Decision Process (MDP), defined by the tuple $\langle \mathcal{S}, \mathcal{A}, \mathcal{P}, \mathcal{R}, \gamma \rangle$ such that \mathcal{S} is the finite set of states, \mathcal{A} is the finite set of actions, \mathcal{P} is the state transition probability matrix with elements $\mathcal{P}_{ss'}^a = P[S_{t+1} = s' | S_t = s, A_t = a]$, \mathcal{R} is the reward function with $\mathcal{R}_s^a = E[R_{t+1} | S_t = s, A_t = a]$, and $\gamma \in [0, 1)$ is the discount factor. More precisely, at each time step t , the agent interacts with the environment, observes the state S_t , takes an action A_t , receives a reward R_{t+1} , and moves to state S_{t+1} according to \mathcal{P} . The goal of the agent is to find the optimal policy π^* that maximizes the infinite-horizon expected return G_t , defined as the sum of the discounted rewards from time t . Specifically, G_t is defined as

$$G_t = \sum_{\tau=0}^{+\infty} \gamma^\tau R_{t+\tau}. \quad (1)$$

In the case of a Partially Observable MDP (POMDP), the agent only perceives an observation O_t of S_t , which provides partial information about the underlying state S_t .

Various algorithms have been developed to determine π^* . While in our previous work we focused on single-agent policy-based RL algorithms, in this paper we extend the analysis to consider a multi-agent approach (MARL), as described in Sec. III-A. Then, in Secs. III-B and III-C we present our MARL and scheduling algorithms, respectively.

A. Formalization of the Model

A centralized MARL problem is characterized by N agents, where each agent aims at maximizing its own total expected return, while interacting with the other agents in a dynamic environment. However, in this approach, the size of the action space grows exponentially with the number of agents [18]. To address this challenge, the problem is decomposed into a smaller and more tractable decentralized decision problem. Specifically, we consider a Decentralized POMDP (Dec-POMDP) [19], i.e., a multi-agent extension of a POMDP. It is defined as a tuple $\langle \mathcal{N}, \mathcal{S}, \{\mathcal{A}_i\}_{i \in \mathcal{N}}, \{\mathcal{O}_i\}_{i \in \mathcal{N}}, \mathcal{P}, \mathcal{R}, \gamma \rangle$, where \mathcal{N} is a finite set of agents, \mathcal{S} is a finite set of states, \mathcal{A}_i is the finite set of actions for agent $i \in \mathcal{N}$, \mathcal{O}_i is the finite set of observations for agent $i \in \mathcal{N}$, $\mathcal{P} : \mathcal{S} \times \mathcal{A}_{\mathcal{N}} \times \mathcal{S} \rightarrow [0, 1]$ is a state transition probability function, and $\mathcal{R} : \mathcal{S} \times \mathcal{A}_{\mathcal{N}} \rightarrow \mathbb{R}$ is the reward function. Each agent learns its decentralized policy, utilizing only its local observations and rewards, while interacting with the shared environment.

Notably, the RAN-AI entity described in Sec. II-A can be modeled as an MARL problem, and framed into a Dec-POMDP model. We provide the following definitions of state \mathcal{S} , observation \mathcal{O} , action \mathcal{A} and reward \mathcal{R} .

a) State and observation: The state (observation) is defined as a set of network measurements from all UEs (from a single UE). These measurements are gathered by the RAN-AI in the gNB through dedicated control signals during data transmissions. Specifically, the state/observation consists of the following metrics: the average SINR, the UL buffer size, the number of OFDM symbols required to transmit the data in the

UL buffer (given the Modulation and Coding Scheme (MCS)), the average MCS index, and the average E2E latency and number of bytes transmitted at the application layer.

b) Action: The action space \mathcal{A}_i is identical for every UE $_i$, $i \in \mathcal{N}$. The action is defined as a scalar value $k \in \{1, \dots, K\}$ corresponding to the priority level assigned to UE $_i$ at each resource allocation opportunity (see Sec. II-B).

c) Reward: The reward function is designed to indicate if latency requirements are satisfied by a certain UE. Specifically, a positive reward is returned if the E2E latency ℓ at the application layer is lower than or equal to a predefined threshold τ ; otherwise, the reward is a penalization proportional to the violation of τ . So, the reward function is defined as:

$$R = \begin{cases} 1 & \text{if } \ell \leq \tau, \\ -(\ell - \tau)/100 & \text{otherwise.} \end{cases} \quad (2)$$

B. MARL Algorithms

We consider a PPO algorithm for the training of the RAN-AI [20] since, contrary to more traditional methods like Q-learning, it is more suitable to manage non-stationary multi-agent environments as the size of the network, i.e., the number of agents/UEs, increases. Specifically, PPO is a model-free method derived from the Trust Region Policy Optimization (TRPO) algorithm [21], which alternates between interaction with the environment and optimization (in multiple epochs) of a clipped surrogate objective function using Stochastic Gradient Descent (SGD). Let $r_t(\theta) = \pi_\theta(a_t | o_t) / \pi_{\theta_o}(a_t | o_t)$ be the probability ratio measuring the divergence between an updated parameterized policy π_θ and the original policy π_{θ_o} (i.e., before the most recent parameters update). Then, let \hat{A}_t be an estimator of the advantage function at time t , defined as the difference between the state-action value function (i.e., the Q -function) and the state value function. The clipped objective function can be written as

$$L^{\text{CL}}(\theta) = \mathbb{E}_t \left[\min \left(r_t(\theta) \hat{A}_t, \text{clip}(r_t(\theta), 1 - \epsilon, 1 + \epsilon) \hat{A}_t \right) \right] \quad (3)$$

where ϵ is an hyperparameter.

Moreover, since in PPO a state value function approximator V_ϕ is implemented and exploration is encouraged, the final objective function becomes

$$L(\theta, \phi) = L^{\text{CL}}(\theta) - c_1 L^{\text{VF}}(\phi) + c_2 S(\pi_\theta), \quad (4)$$

where L^{VF} is the mean squared error between V_ϕ and the target return G_t , and $S(\pi_\theta)$ represents the entropy of the policy. Constants c_1 and c_2 are hyperparameters that balance the contribution of the two terms.

The implementation of this model involves two NNs, i.e., a policy network π_θ (actor) and a value network V_ϕ (critic). The former represents the policy of the agent; indeed, it receives as input the state and gives as output a probability distribution over the action space. The latter represents the state value function, and contributes to reducing the variance of the advantage function, i.e., of the gradient estimates. The NNs are fully connected: for π_θ , we have $|\mathcal{O}_i|$ input neurons and $|\mathcal{A}_i|$ output neurons; for V_ϕ , we have $|\mathcal{O}_i|$ input neurons and

a single output neuron. There are two fully-connected hidden layers with n_N neurons each, using the hyperbolic tangent as activation function, except for the output layer of π_θ where the softmax function is adopted. The parameters of the NNs are updated using the Adam algorithm, with a learning rate α . During the training, PPO is executed to generate trajectories of a fixed length of T steps, which are tuples of states, actions and rewards collected interacting with the environment. During the learning, these trajectories are split into mini-batches of size M to compute the gradient for improving the stability.

The Generalized Advantage Estimation (GAE) [22] technique is used to approximate the advantage function \hat{A}_t . Notably, we use parameter $\lambda \in [0, 1]$ to control the trade-off between bias (due to systematic errors in the estimation of \hat{A}_t) and variance (due to noise in long trajectories). Formally, the advantage function at time t is computed as

$$\hat{A}_t = \sum_{l=0}^{T-t} (\gamma\lambda)^l \delta_{t+l}, \quad (5)$$

where $\delta_t = r_t + \gamma V(s_{t+1}) - V(s_t)$ is the temporal difference error at time t .

In this paper, we explore two PPO implementations.

a) Independent PPO (IPPO): IPPO [23] is the multi-agent version of PPO where N decentralized and independent policies are learnt by using only local observations. Therefore, the MARL problem involving N agents is decomposed into N single-agent problems. This approach is very effective and scalable, but does not guarantee learning stability or convergence to the optimal policy. In fact, from the point of view of an agent, the simultaneous learning process of the other agents introduces additional dynamics that may compromise the stationarity of the environment.

b) Multi-Agent PPO (MAPPO): MAPPO [24] is an example of a centralized training with decentralized execution (CTDE) framework in which model parameters are shared to efficiently collect information in a centralized fashion [25]. Instead of having isolated agents, this approach updates a single actor and a single critic using data gathered from all N agents. Therefore, all agents share the same policy and value function network. This technique accelerates the learning, is easy to implement, and more scalable with the number of agents than other CTDE approaches [25]. However, since observations come from multiple agents, the estimates of the advantage function have a high variance, making the system unstable and more difficult to generalize.

C. Scheduling Algorithms

Our scheduling approach is to allocate, for each UE, a certain number of OFDM symbols per slot based on the priority level k (i.e., the action of the MARL algorithm based on IPPO or MAPPO). Notably, we implement two strategies.

a) Proportional Allocation (PA): The number of OFDM symbols u_i allocated to UE $_i$, $i \in \{1, \dots, N\}$, is computed as

$$u_i = \left\lfloor U \frac{k_i}{\sum_{i \in \mathcal{N}} k_i} \right\rfloor, \quad (6)$$

TABLE I: Simulation parameters.

Parameter	Value
Number of UEs/agents (N)	{3, 5, 8}
Carrier frequency (f_c)	28 GHz
Bandwidth (B)	50 MHz
Available OFDM symbols/slot (U)	12
LiDAR frame rate (f)	30 fps
Latency threshold (τ)	{15, 25, 35} ms
Number of priority levels (K)	3
Discount factor (γ)	0.95
GAE parameter (λ)	0.95
Number of neurons in hidden layers (n_N)	64
Learning rate (α)	10^{-4}
Hyperparameters ($\{\epsilon, c_1, c_2\}$)	{0.2, 0.5, 0.01}
Length of a trajectory (T)	512 steps
Mini-batch size (M)	64 steps

where U is the number of available OFDM symbols/slot. If $u_i < U$, the remaining OFDM symbols in the slot are used to serve other UE transmissions, starting from the UE(s) with the highest priority. Therefore, a principle of fairness is preserved.

b) Greedy Allocation (GA): The allocation of OFDM symbols within a slot is greedy with respect to the priority level. Specifically, all U symbols are assigned to the UE with the absolute highest priority. Unallocated symbols, if any, are assigned to the next UE(s) with higher priority. This procedure is repeated iteratively until the slot is completely allocated.

For both PA and GA, the allocation of resources is upper bounded by the number of symbols required to transmit the actual content (data) of the buffer of each UE, given the MCS.

IV. PERFORMANCE EVALUATION

In this section, we first describe our simulation parameters (Sec. IV-A), then we present our numerical results (Sec. IV-B).

A. Simulation Parameters

Our simulation scenario is implemented in ns-3, a system-level, end-to-end, scalable, and open-access simulator of wireless networks. Notably, ns-3 comes with a dedicated module to simulate and test ML/RL algorithms within the RAN [16] based on the pipeline described in Sec. II, that we extended to implement our MARL IPPO and MAPPO approaches.² Simulation parameters are reported in Table I, and described below.

a) Communication: We consider 5G NR communication between the gNB and the UE(s) at a carrier frequency f_c of 28 GHz and with a bandwidth B of 50 MHz, so as to maximize the channel capacity. The 5G NR slot consists of $U = 12$ available OFDM symbols, given that the first 2 symbols are reserved for control in UL and DL. We use numerology 3, so the resulting OFDM symbol duration is 8.92 μ s. The gNB (UE) has a transmission power of 30 (23) dBm. The (ideal) wired channel has a propagation delay of 10 ms and a transfer data rate of 100 Gbps.

²Source code: <https://github.com/signetlabdei/ns3-ran-ai>.

b) *Application*: We consider an application generating LiDAR point clouds at a rate $f = 30$ fps. For simplicity, we restrict our analysis to a (representative) subset of Draco compression configurations (q, c) , with $q \in \{8, 9, 10\}$ and $c \in \{0, 5, 10\}$. Specifically, $(8, 0)$ is the most aggressive configuration, resulting in a compressed data size that is roughly half of the most conservative configuration $(10, 10)$.

c) *Learning algorithm*: For the policy network π_θ , we consider 6 input neurons equal to the size of the state/observation space, and K output neurons equal to the size of the action space, i.e., the number of scheduling priority levels. We empirically set $K = 3$ based on offline simulations: a smaller K would be insufficient to properly differentiate UEs, while increasing K could lead to a complex and/or unstable learning environment, especially when the number of priority levels approximates that of the UEs. Our MARL algorithms are trained on 250 episodes with 400 learning steps for every UE/agent. Each episode is an independent simulation in ns-3, where 400 transmissions of point clouds are performed. The rest of the learning parameters are reported in Table I.

d) *Benchmarks*: We compare the performance of IPPO vs. MAPPO, using either PA or GA for resource allocation, for a total of 4 combinations. For comparison, we consider an RR benchmark in which UEs are assigned the same number of resources, regardless of the priority level, so independent of the actual latency conditions.

e) *Metrics*: We run 250 independent ns-3 simulations, and evaluate: (i) the average E2E latency at the application layer, measured from the time at which a data packet is generated at the transmitter to the time it is received; (ii) the average reward over the episodes; and (iii) the average latency-success probability, that is the probability that the latency is lower than or equal to a threshold τ , i.e., $P_{\ell \leq \tau}$. We investigate the impact of the number of vehicles N , the compression configuration (q, c) , and the latency threshold τ .

B. Numerical Results

a) *Learning results*: In Fig. 1 we compare the learning performance of IPPO and MAPPO in terms of reward. As expected, MAPPO, despite the increased complexity, generally achieves a higher reward than IPPO with both PA and GA scheduling options, given that the learning parameters are shared to a centralized node and optimized accordingly. Indeed, priorities for each vehicle are computed from a global perspective, resulting in a better coordination among the agents. More precisely, MAPPO demonstrates a more significant performance improvement in PA than in GA due to the inherently more complex nature of the former approach. In GA, the learning is relatively straightforward, involving the identification of the most critical UE to allocate all of the available resources. Conversely, PA requires the allocation of resources among multiple UEs based on their priority levels, which requires strong coordination. In this sense, the collaborative nature of MAPPO facilitates this coordination, compared to an independent approach like IPPO, and can accelerate the convergence of the learning process for PA.

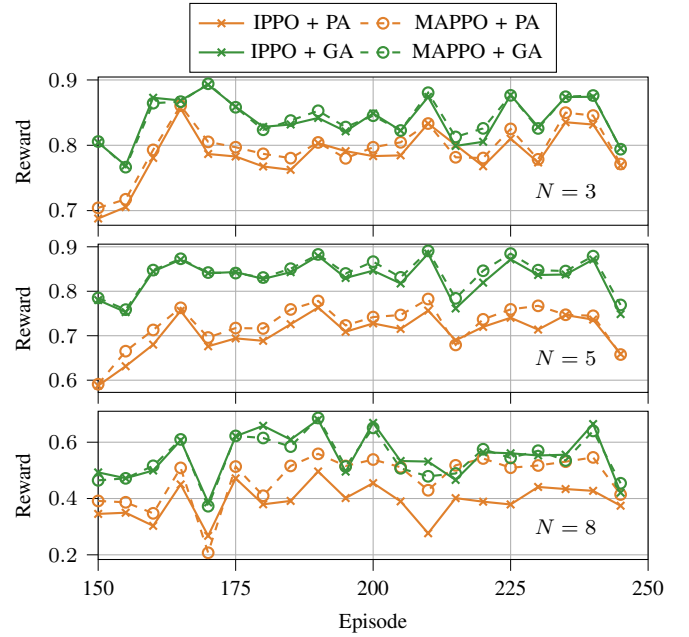


Fig. 1: Average reward at the end of the training for IPPO and MAPPO, combined with PA or GA, for $N \in \{3, 5, 8\}$.

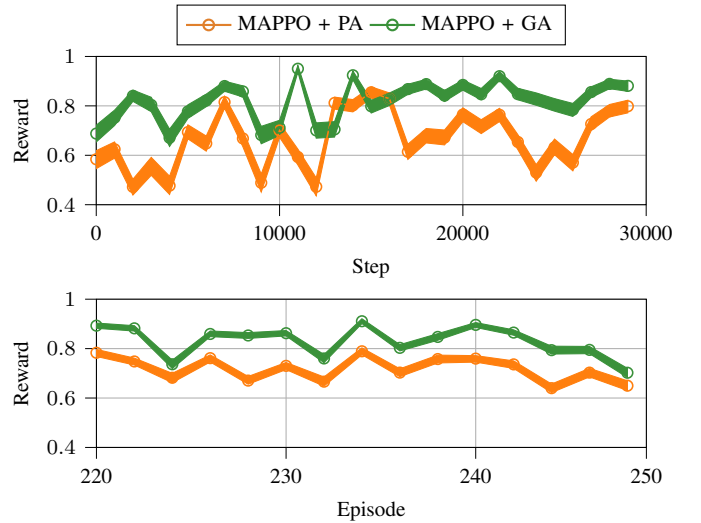


Fig. 2: Average reward at the beginning (top) and at end of the training (bottom) for MAPPO, with $N = 5$.

Moreover, the gap between IPPO and MAPPO increases as N increases, especially for PA. Indeed, in crowded networks, the scheduling complexity increases, and requires more coordination among the agents to efficiently distribute resources, as promoted by MAPPO.

In view of the above results, in the rest of this section we continue our analysis considering only the MAPPO algorithm.

In Fig. 2 we plot the evolution of the reward during the training of MAPPO, focusing on the case of $N = 5$. In particular, at the beginning of the learning process, i.e., over the first 30k steps (15 episodes), the reward improves for both PA and GA algorithms as the training progresses. Eventually, at the end of the training, i.e., in the last 30 episodes, MAPPO

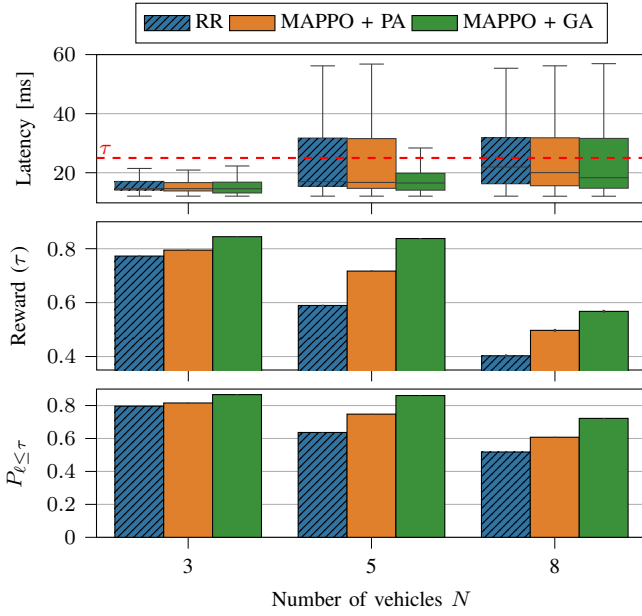


Fig. 3: Average latency, reward and latency-success probability vs. N at the end of the training, for $(q, c) = (8, 0)$ and $\tau = 25$ ms.

with GA achieves a higher reward (0.8) with less variance in comparison to the PA approach (0.7).

b) Impact of the number of UEs: In general, MAPPO outperforms a traditional RR approach in terms of network performance. Specifically, we evaluate the average latency and the latency-success probability $P_{\ell \leq \tau}$.

In Fig. 3 we illustrate the average latency, reward, and the latency-success probability as a function of N at the end of the training. We observe that, while the median latency is always lower than τ with the current settings, its distribution depends on both N and the scheduling approach. As N increases, network congestion also increases, and so does the average (and variance of the) latency. Specifically, with only $N = 3$, the rewards for RR and MAPPO (with both PA and GA options) are very similar and close to 0.8. In this scenario, traffic requests can be easily handled, and network resources can be allocated without the need for coordination or more complex learning-based optimizations. In this sense, RR represents a simple and effective approach to support low latency.

Increasing N , and therefore the channel occupation, MAPPO consistently outperforms RR, which demonstrates the benefits of MARL for resource allocation in a more complex, delay-critical scenario. For example, for $N = 5$, the latency-success probability is around 35% (15%) higher with MAPPO using GA (PA) compared to the RR benchmark. This trend also appears from the boxplot in Fig. 3 (top), where RR and MAPPO with PA exhibit a significantly higher number of latency violations than MAPPO with GA, even though the median latency remains below τ . In fact, as discussed, MAPPO with GA outperforms its PA counterpart as it prioritizes the most constrained UE (in terms of latency) by allocating more

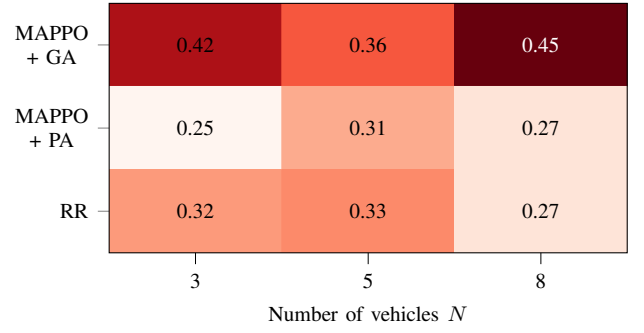


Fig. 4: The 95-percentile of the latency-violation probability vs. N .

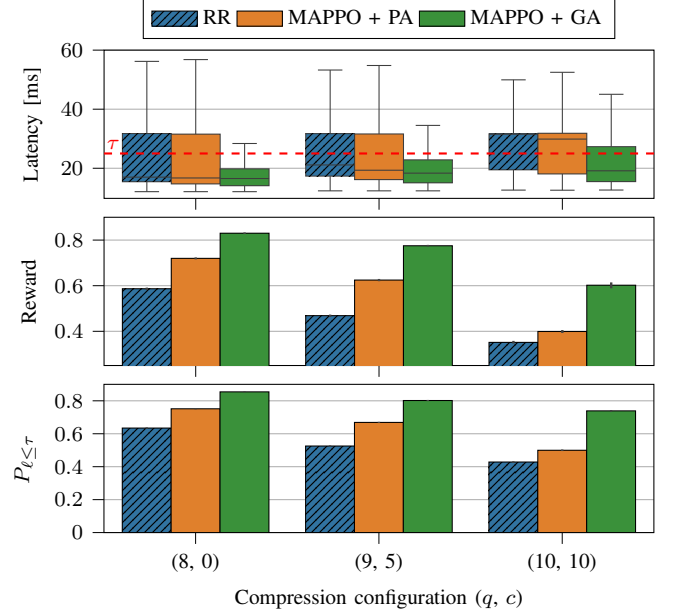


Fig. 5: Average latency, reward and latency-success probability vs. the compression configuration at the end of the training, for $N = 5$ and $\tau = 25$ ms.

network resources, at the expense of the others. Meanwhile, PA involves a principle of fairness by modulating the number of allocated resources to satisfy as many UE requests as possible. Focusing on worst-case latency, in Fig. 4 we plot the 95-th percentile of the latency-violation probability, i.e., $P_{\ell > \tau}$, vs. N , and as a function of the scheduling approach. We clearly see that MAPPO with GA yields the worst performance in this regard, since it aggressively prioritizes a limited subset of UEs, depriving others of sufficient channel resources. Conversely, PA mitigates this negative condition, although it suffers from a higher average latency.

Finally, as N continues to increase, all scheduling solutions converge to similar average latency performance. In this congested scenario, the primary bottleneck of the system is represented by the limited number of resources, which are insufficient to accommodate all traffic requests, regardless of the underlying scheduling implementation. Nevertheless, MAPPO still outperforms RR in terms of reward and latency-success probability, and represents a more robust and scalable solution as N increases.

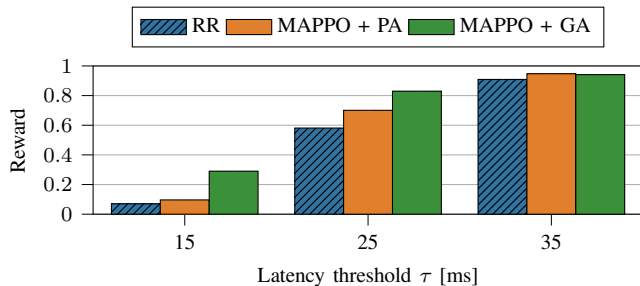


Fig. 6: Average reward at the end of the training vs. τ , for $N = 5$ and $(q, c) = (8, 0)$.

c) *Impact of the compression configuration:* The compression configuration directly determines the size of the LiDAR point clouds to be transmitted, and therefore the data rate of the application. For example, for $(q, c) = (10, 10)$, the resulting aggregated data rate for $N = 8$ is 66.2 Mbps at a frame rate $f = 30$ fps. At the end of the training, Fig. 5 shows that the average reward is inversely proportional to the level of data compression, dropping below 0.6 for $(q, c) = (10, 10)$, even after optimization with MAPPO. This is because lower compression results in higher data rates, making latency constraints more difficult to satisfy.³ Nevertheless, MAPPO consistently outperforms the benchmark RR approach. Notably, under the most conservative compression configuration (i.e., $(q, c) = (10, 10)$), MAPPO with GA is the only approach capable of reducing the median latency below τ , and satisfy latency constraints for more than 70% of the time, vs. 50% and 42% for MAPPO with PA and RR, respectively.

d) *Impact of the latency threshold:* Finally, in Fig. 6 we analyze the reward as a function of τ . In general, the reward decreases as τ decreases. For example, with $\tau = 15$ ms, MAPPO with GA outperforms RR by 0.2 (+95%) in terms of reward, and stands out as the best scheduling approach in the most challenging environments. With $\tau = 25$ ms, vehicles have more time to complete data transmission before violating the latency constraint, so the gap between MAPPO and RR is limited to +35%. Still, MAPPO with GA continues to be the best scheduler implementation, with an average reward around 0.8. As τ reaches 35 ms, all scheduling options provide comparable performance since the system is no longer heavily constrained, and resources can be efficiently allocated without requiring learning-based optimizations. This scenario is similar to the case of $N = 3$ in Fig. 2, where we demonstrated that, when the network is underutilized, MAPPO does not provide significant performance improvements over simpler approaches like RR.

V. CONCLUSIONS AND FUTURE WORK

In this work we proposed MARL-based scheduling algorithms to support low latency in a TD scenario in the context of PQoS. Specifically, we formalized a multi-agent model,

³Notice that, while higher compression reduces the data rate and network congestion, it may inevitably degrade the quality of data. This analysis is out of the scope of this paper, and was already partially addressed in [6], [8].

and optimized the allocation of radio resources, i.e., OFDM symbols per slot, to minimize the probability of violating some predefined latency constraints. We evaluated two multi-agent extensions of PPO, i.e., MAPPO and IPPO, together with a proportional and a greedy strategy to distribute OFDM symbols based on priority levels. To assess the performance of our proposed scheduler models, we run a simulation campaign in ns-3, using RR as a benchmark. We showed that MAPPO outperforms IPPO due to the fact that agents coordinate and share measurements with the network during the learning phase. In particular, MAPPO with GA achieves lower average latency than its PA counterpart, and stands out as the most robust and effective scheduling approach, especially in the most constrained network configurations, e.g., when the number of vehicles and/or the application data rate increase. However, many severe latency violations are experienced, while PA promotes fairness in resources allocation.

As part of our future work, we plan to further extend our MARL framework by incorporating additional parameters, including the impact of compression on data quality and energy consumption, together with performance metrics such as throughput and latency.

REFERENCES

- [1] M. Giordani, M. Polese, M. Mezzavilla, S. Rangan, and M. Zorzi, "Toward 6G Networks: Use Cases and Technologies," *IEEE Communications Magazine*, vol. 58, no. 3, pp. 55–61, Mar. 2020.
- [2] T. Zhang, "Toward automated vehicle teleoperation: Vision, opportunities, and challenges," *IEEE Internet of Things Journal*, vol. 7, no. 12, pp. 11 347–11 354, Dec. 2020.
- [3] 5GAA, "C-V2X Use Cases Volume II: Examples and Service Level Requirements," White Paper, 2020.
- [4] J. Choi, V. Va, N. Gonzalez-Prelcic, R. Daniels, C. R. Bhat, and R. W. Heath, "Millimeter-wave vehicular communication to support massive automotive sensing," *IEEE Communications Magazine*, vol. 54, no. 12, pp. 160–167, Dec. 2016.
- [5] M. Boban, M. Giordani, and M. Zorzi, "Predictive Quality of Service (PQoS): The Next Frontier for Fully Autonomous Systems," *IEEE Network*, vol. 35, no. 6, pp. 104–110, Nov/Dec 2021.
- [6] F. Mason, M. Drago, T. Zugno, M. Giordani, M. Boban, and M. Zorzi, "A Reinforcement Learning Framework for PQoS in a Teleoperated Driving Scenario," in *IEEE Wireless Communications and Networking Conference (WCNC)*, 2022.
- [7] F. Bragato, T. Lotta, G. Ventura, M. Drago, F. Mason, M. Giordani, and M. Zorzi, "Towards Decentralized Predictive Quality of Service in Next-Generation Vehicular Networks," in *IEEE Information Theory and Applications Workshop (ITA)*, 2023.
- [8] F. Bragato, M. Giordani, and M. Zorzi, "Federated Reinforcement Learning to Optimize Teleoperated Driving Networks," in *IEEE Global Communications Conference*, 2024. [Online]. Available: <https://arxiv.org/abs/2410.02312>
- [9] L. Liang, H. Ye, G. Yu, and G. Y. Li, "Deep-Learning-Based Wireless Resource Allocation With Application to Vehicular Networks," *Proceedings of the IEEE*, vol. 108, no. 2, pp. 341–356, Feb. 2020.
- [10] Z. Gu, C. She, W. Hardjawana, S. Lumb, D. McKechnie, T. Essery, and B. Vucetic, "Knowledge-Assisted Deep Reinforcement Learning in 5G Scheduler Design: From Theoretical Framework to Implementation," *IEEE Journal on Selected Areas in Communications*, vol. 39, no. 7, pp. 2014–2028, Jul. 2021.
- [11] Q. Huang and M. Kadoch, "5G Resource Scheduling for Low-latency Communication: A Reinforcement Learning Approach," in *IEEE 92nd Vehicular Technology Conference (VTC2020-Fall)*, 2020.
- [12] M. Mezzavilla, M. Zhang, M. Polese, R. Ford, S. Dutta, S. Rangan, and M. Zorzi, "End-to-End Simulation of 5G mmWave Networks," *IEEE Communications Surveys & Tutorials*, vol. 20, no. 3, pp. 2237–2263, Thirdquarter 2018.

- [13] D. Krajewicz, J. Erdmann, M. Behrisch, and L. Bieker, "Recent development and applications of SUMO - Simulation of Urban MObility," *International Journal On Advances in Systems and Measurements*, vol. 5, no. 3&4, pp. 128–138, Dec. 2012.
- [14] M. Boban, J. Barros, and O. K. Tonguz, "Geometry-based vehicle-to-vehicle channel modeling for large-scale simulation," *IEEE Transactions on Vehicular Technology*, vol. 63, no. 9, pp. 4146–4164, Nov. 2014.
- [15] Google. (2017) Draco 3D Data Compression. [Online]. Available: <https://google.github.io/draco/>
- [16] M. Drago, T. Zugno, F. Mason, M. Giordani, M. Boban, and M. Zorzi, "Artificial Intelligence in Vehicular Wireless Networks: A Case Study Using ns-3," in *Proceedings of the 2022 ACM Workshop on Ns-3*, 2022.
- [17] 3GPP, "NR and NG-RAN Overall Description (Release 15)," *TS 38.300*, 2018.
- [18] S. V. Albrecht, F. Christianos, and L. Schäfer, *Multi-Agent Reinforcement Learning: Foundations and Modern Approaches*. MIT Press, 2024.
- [19] D. S. Bernstein, S. Zilberstein, and N. Immerman, "The complexity of decentralized control of Markov decision processes," in *Proceedings of the Sixteenth Conference on Uncertainty in Artificial Intelligence*, 2000.
- [20] J. Schulman, F. Wolski, P. Dhariwal, A. Radford, and O. Klimov, "Proximal policy optimization algorithms," 2017. [Online]. Available: <https://arxiv.org/abs/1707.06347>
- [21] J. Schulman, S. Levine, P. Abbeel, M. Jordan, and P. Moritz, "Trust region policy optimization," in *Proceedings of the 32nd International Conference on Machine Learning*, 2015.
- [22] J. Schulman, P. Moritz, S. Levine, M. Jordan, and P. Abbeel, "High-dimensional continuous control using generalized advantage estimation," in *Proceedings of the International Conference on Learning Representations (ICLR)*, 2016.
- [23] C. S. de Witt, T. Gupta, D. Makoviichuk, V. Makoviyuchuk, P. H. S. Torr, M. Sun, and S. Whiteson, "Is independent learning all you need in the starcraft multi-agent challenge?" 2020. [Online]. Available: <https://arxiv.org/abs/2011.09533>
- [24] C. Yu, A. Velu, E. Vinitzky, J. Gao, Y. Wang, A. Bayen, and Y. Wu, "The surprising effectiveness of PPO in cooperative multi-agent games," in *Proceedings of the 36th International Conference on Neural Information Processing Systems*, 2022.
- [25] C. Amato, "An introduction to centralized training for decentralized execution in cooperative multi-agent reinforcement learning," 2024. [Online]. Available: <https://arxiv.org/abs/2409.03052>